ACS APPLIED MATERIALS & INTERFACES
Research Article
www.acsami.org

Boron-Doped Peroxo-Zirconium Oxide Dielectric for High-Performance, Low-Temperature, Solution-Processed Indium Oxide Thin-Film Transistor

Jee Ho Park, Young Bum Yoo, Keun Ho Lee, Woo Soon Jang, Jin Young Oh, Soo Sang Chae, Hyun Woo Lee, Sun Woong Han, and Hong Koo Baik*

Department of Materials Science and Engineering, Yonsei University, 50 Yonsei-ro, Seodaemun-gu, Seoul 120-749, South Korea

Supporting Information

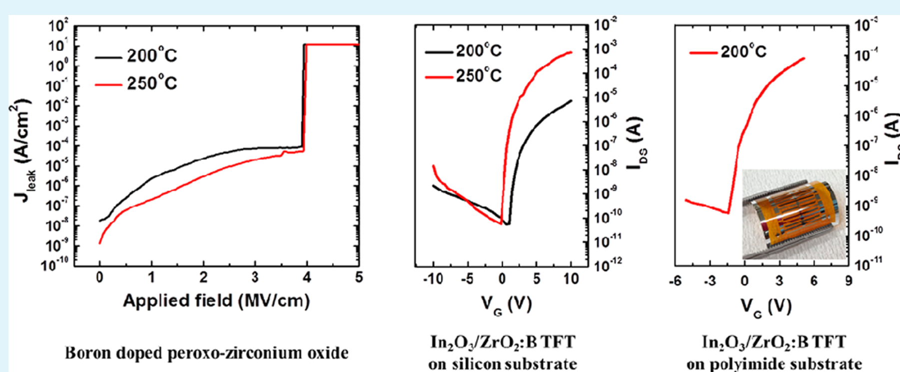

ABSTRACT: We developed a solution-processed indium oxide (In_2O_3) thin-film transistor (TFT) with a boron-doped peroxo-zirconium (ZrO_2:B) dielectric on silicon as well as polyimide substrate at 200 °C, using water as the solvent for the In_2O_3 precursor. The formation of In_2O_3 and ZrO_2:B films were intensively studied by thermogravimetric differential thermal analysis (TG-DTA), attenuated total reflectance Fourier transform infrared spectroscopy (ATR-FT IR), high-resolution X-ray diffraction (HR-XRD), and X-ray photoelectron spectroscopy (XPS). Boron was selected as a dopant to make a denser ZrO_2 film. The ZrO_2:B film effectively blocked the leakage current at 200 °C with high breakdown strength. To evaluate the ZrO_2:B film as a gate dielectric, we fabricated In_2O_3 TFTs on the ZrO_2:B dielectrics with silicon substrates and annealed the resulting samples at 200 and 250 °C. The resulting mobilities were 1.25 and 39.3 $cm^2/(V\ s)$, respectively. Finally, we realized a flexible In_2O_3 TFT with the ZrO_2:B dielectric on a polyimide substrate at 200 °C, and it successfully operated a switching device with a mobility of 4.01 $cm^2/(V\ s)$. Our results suggest that aqueous solution-processed In_2O_3 TFTs on ZrO_2:B dielectrics could potentially be used for low-cost, low-temperature, and high-performance flexible devices.

KEYWORDS: *aqueous solution process, boron-doped peroxo-zirconium, thin-film transistor, hydrogen peroxide, indium oxide*

1. INTRODUCTION

Metal oxides are fascinating materials because of their versatile characteristics such as piezoelectricity, superconductivity, semiconductivity, and ferroelectricity.[1−4] Thus, they are used in various applications such as nanogenerators, solar cells, batteries, and thin-film transistors (TFTs).[5−8] In particular, TFTs using a metal oxide semiconductor such as zinc tin oxide (ZTO), indium zinc oxide (IZO), indium gallium zinc oxide (IGZO), gallium indium oxide (GIO), and indium oxide (In_2O_3) as the channel layer are an emerging area of research in the flat panel display industry because of their high mobility even in an amorphous phase, high transparency, high stability, and large-area uniformity.[9−13] Among the various deposition methods such as radio frequency sputtering, chemical vapor deposition (CVD), atomic layer deposition (ALD), inkjet printing, and spin-coating, solution processing is becoming a useful deposition technique because of its simplicity, low cost, easy controllability of chemical stoichiometry, and mass productivity. Thus, enormous efforts have been made to fabricate metal oxide films via solution processing. However, fabricating metal oxide films using solution processing requires a high annealing temperature of above 450 °C because of the high pyrolysis and dehydroxylation temperatures of typical precursors, which restrict substrate selectivity. To resolve this problem, researchers have explored a variety of methods. However, most of these studies evaluated the electrical properties of the metal oxide TFT on thermally grown SiO_2 or on a vacuum-deposited metal oxide dielectric.[14−17] To realize a full solution process, both the channel and the dielectric layer should be formed by solution processing. Thus,

Received: June 4, 2013
Accepted: July 25, 2013
Published: July 25, 2013

ACS Publications © 2013 American Chemical Society

solution-processed dielectric materials formed at low temperature have also been investigated. However, it is difficult to fabricate a metal oxide dielectric with low leakage current density and high breakdown strength at low annealing temperatures. Several groups have developed solution-processed dielectrics at low temperatures of approximately 350 °C and evaluated the resulting TFT properties. For example, Kim et al. reported an IGZO TFT with an $AlPO_4$ dielectric that had a low leakage current with high breakdown strength and a mobility of 4.5 $cm^2/(V\ s)$ at 350 °C.[18] Avis et al. demonstrated a solution-processed ZTO TFT on a solution-processed hafnium oxide dielectric.[19] The resulting TFT had a smooth surface and a dielectric constant of 14 at a maximum temperature of 300 °C with a mobility of 1.05 $cm^2/V{\cdot}s$. Kim et al. introduced high-pressure annealing for dense zirconium oxide and showed an IZO TFT on a ZrO_2 dielectric with a mobility of 0.1 $cm^2/(V\ s)$ at 350 °C.[20] In addition, we recently demonstrated a solution-processed IZO TFT with a highly dense peroxo-ZrO_2 dielectric.[10] This TFT had a smooth surface, low leakage current, a high dielectric constant of 14.8, and a mobility of 7.21 $cm^2/(V\ s)$ at 350 °C. Moreover, we realized completely solution-processed IZO TFTs on ITO:F-coated glass substrates by combining a stacked $ZrO_2/Al_2O_3/ZrO_2$ (ZAZ) gate dielectric with spray-coated single-walled carbon nanotube (SWCNT) source and drain electrodes at 350 °C.[21] The stacked ZAZ dielectric effectively blocked the leakage current and showed a high breakdown strength. The integrated TFT showed a mobility of 0.45 $cm^2/(V\ s)$ with an optical transparency of 76.5%.

The 350 °C annealing temperature, which is conventionally used in the flat panel display industry, limits development to the use of glass or silicon substrates. To realize the fabrication of a solution-processed TFT on a flexible polymer substrate such as polyethersulfone (PES) and polyimide (PI), the annealing temperature should be reduced to below 200 °C. Some researchers have reported forming a dielectric material using a solution process at 150 °C on a silicon substrate with a conventionally used ZnO channel layer derived from a $Zn(OH)_x(NH_3)_y^{(2-x)+}$ precursor.[22−24]

In this study, we fabricated a solution-processed In_2O_3 TFT with a boron-doped peroxo-zirconium oxide dielectric at a maximum temperature of 200 °C on a silicon substrate without any post-treatment. Moreover, we realized an In_2O_3 TFT with a boron-doped peroxo-zirconium oxide dielectric on a flexible PI substrate. The saturation mobilities of the In_2O_3 TFTs with boron-doped peroxo-zirconium oxide dielectrics on silicon substrates annealed at 200 and 250 °C were 1.25 and 39.3 $cm^2/(V\ s)$, respectively. The flexible TFT had a mobility of 4.01 $cm^2/(V\ s)$, a threshold voltage (V_{th}) of 0.28 V, and an on/off current ratio ($I_{on/off}$) of 1.68×10^5. The In_2O_3 and boron-doped peroxo-zirconium oxide materials used in this study were analyzed with various tools, and their properties and electrical characteristics were studied.

To accomplish a solution-processed TFT at 200 °C, we performed material design and developed two strategies. First, we adopted water as the solvent for channel layer precursor instead of the conventionally used 2-methoxyethnaol in order to exclude carbonyl groups, which decompose at approximately 300 °C. In addition, water molecules directly solvate metal ions and perform a hydrolysis reaction, thus producing a metal hydroxide. These metal hydroxides react with adjacent metal hydroxides and develop a metal−oxygen−metal frame, which results in the formation of a metal oxide at low temperature. Second, we selected boron as a dopant for the peroxo-zirconium oxide gate dielectric because of its small ion radius and high B−O bonding energy. This boron dopant increased the density of the peroxo-zirconium oxide and effectively blocked the leakage current at low temperature. Finally, we integrated In_2O_3 TFTs on ZrO_2:B dielectrics on silicon and PI substrates at 200 °C.

2. EXPERIMENTAL SECTION

2.1. Synthesis of In_2O_3 and Boron-Doped ZrO_2 solutions. For the In_2O_3 solution, 0.1 M indium nitrate hydrate [$In(NO_3)_3{\cdot}xH_2O$] was dissolved in deionized water. For the boron-doped ZrO_2 solution, 0.2 M zirconium oxychloride octahydrate ($ZrOCl_2{\cdot}8H_2O$) and various mole concentrations (0, 4.7, 9, 16, 33, and 50 mol %) of boric acid (H_3BO_3) were mixed with 2-methoxyethanol. H_2O_2 (6.67 M) was subsequently added. The In_2O_3 and boron-doped ZrO_2 solutions were stirred vigorously for 24 h under ambient conditions and filtered through 0.2 and 0.45 μm polytetrafluoroethylene (PTFE) syringe filters, respectively, before spin-coating. The 9 mol %-boron-doped ZrO_2 film is denoted herein as ZrO_2:B.

2.2. Film Characterization. Thermogravimetric differential thermal analysis (TG-DTA, Seiko Exstar 6000, Seiko) was used to measure the thermal behavior of the In_2O_3 and ZrO_2:B powders, which were dried at 110 °C for 12 h at a heating rate of 8 °C/min from room temperature to 600 °C under ambient conditions. The structures of the In_2O_3 and boron-doped ZrO_2 films, each with a thickness of 100 nm, were measured by high-resolution X-ray diffraction (HR-XRD, Ultima IV, Rigaku) with Cu Kα radiation. The chemical characteristics of the In_2O_3 and ZrO_2:B films were investigated by attenuated total reflectance Fourier transform infrared spectroscopy (ATR-FT IR, Vertex 70, Bruker). The chemical structures of In_2O_3 and ZrO_2:B were examined by X-ray photoelectron spectroscopy (XPS, K-alpha, Thermo UK) using Al Kα radiation (1486.6 eV). A carbon 1s peak at 284.8 eV was used for calibration. The refractive index was measured by spectroscopic ellipsometry (SE MG-Vis 1000, Nano View). Data were collected at an incident angle of 69.7° in the range 350−850 nm. The thickness of the ZrO_2:B/Al/PVP/PI substrate (where PVP is polyvinylphenol) was measured by field-emission scanning electron microscopy (FE-SEM, JSM-7001F, JEOL). The surface morphology of the ZrO_2:B film was investigated by atomic force microscopy (AFM, MFP-3D-SA, Asylum Research).

2.3. Metal−Insulator−Metal Device Fabrication. To measure the electrical characteristics of the ZrO_2:B film, we fabricated metal−insulator−metal (MIM) structures consisting of Al/ZrO_2:B/heavily boron-doped silicon (Si^{++}) substrates. The ZrO_2:B solution was spin-coated onto the Si^{++} substrates at 3000 rpm for 20 s and soft-baked at 150 °C for 5 min. The spin-coating process was repeated five times, after which the samples were hard-baked at either 200 or 250 °C for 2 h under ambient conditions. The thicknesses of the annealed ZrO_2:B films were measured by FE-SEM and spectroscopic ellipsometry and were found to be 165 and 120 nm, respectively. The circular aluminum electrode with 50 nm thickness was deposited by thermal evaporator through shadow metal mask. The area of the circular aluminum electrode was 0.17 mm^2.

2.4. Thin-Film Transistor Device Fabrication. We selected a bottom-gate top-contact structure for the In_2O_3 TFTs on the ZrO_2:B dielectric. The In_2O_3 TFTs on the Si^{++} substrate with thermally grown 200-nm-thick SiO_2 (In_2O_3/SiO_2 TFT) was fabricated by spin-coating the In_2O_3 solution on the substrates at 3000 rpm for 20 s and annealing at various temperatures (200, 230, 250, 300, and 350 °C). The In_2O_3 TFT on Si^{++} substrate with 200 °C- and 250 °C-annealed ZrO_2:B film (In_2O_3/ZrO_2:B TFT) was deposited via spin-coating at 3000 rpm for 20 s and annealed at 200 and 250 °C, respectively. In the case of the flexible TFT, its structure was Al/In_2O_3/ZrO_2:B/Al/PVP/PI. The PVP solution was a mixture of PVP and glycol monomethyl ether acetate (PGMEA), and 10 wt % poly(melamine-co-formaldehyde) was added to this solution. The PVP layer was deposited on the PI substrate via spin-coating at 3000 rpm for 50 s and annealed at 200 °C for 1 h. This PVP layer was formed for planarizing the PI

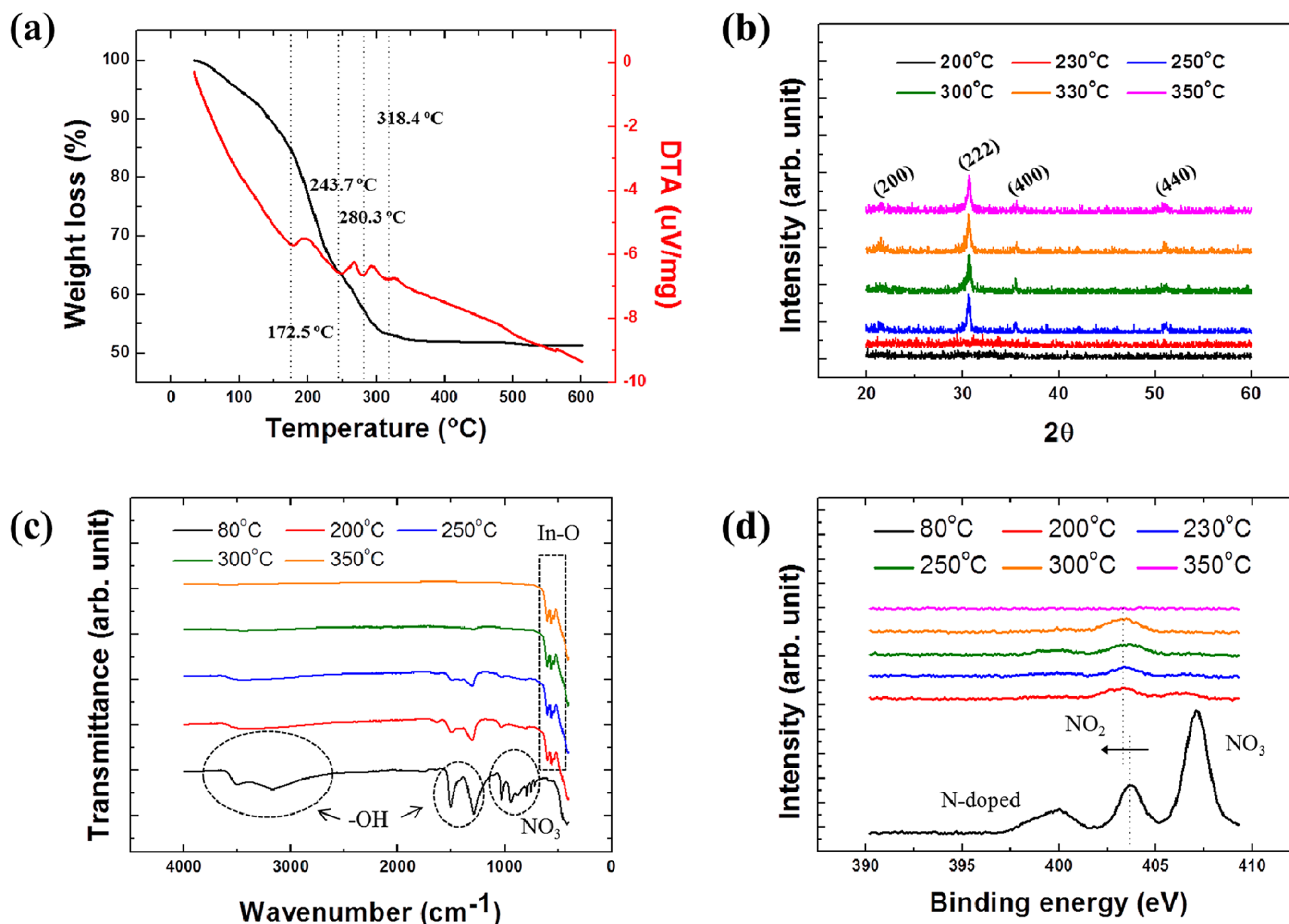

Figure 1. (a) TG-DTA, (b) XRD spectra, (c) FT-IR, and (d) XPS N 1s peak of In_2O_3 with various annealing temperatures.

substrate. The ZrO_2:B was spin-coated on the Al/PVP/PI substrate five times at 3000 rpm for 20 s and annealed at 200 °C for 2 h. The thicknesses of the ZrO_2:B, Al, and PVP layers were 32.5, 67.5, and 240 nm, respectively (see Figure S1 in the Supporting Information). The In_2O_3 film on the ZrO_2:B/Al/PVP/PI substrate was deposited via spin-coating at 3000 rpm for 20 s and annealed at 200 °C for 1 h. The aluminum source/drain electrodes (50 nm thick) were deposited by a thermal evaporator [pressure ~1×10^{-6} Torr (1.33 mPa)] through a shadow mask. The channel width and length were 1000 and 150 μm, respectively. All the chemical compounds were purchased from Sigma-Aldrich.

2.5. Electrical Measurements. The capacitance−frequency of the ZrO_2:B film was measured by an HP 4284A LCR meter in the range 100 Hz−1 MHz. The leakage current density (J_{leak})−applied field (E) characteristics of the ZrO_2:B film were measured by a semiconductor parameter analyzer (Agilent E5270). The electrical properties of In_2O_3 TFTs on the SiO_2/Si^{++}, ZrO_2:B/Si^{++}, and ZrO_2:B/Al/PVP/PI substrates were also measured by a semiconductor parameter analyzer (Agilent E5270) at room temperature in the dark.

3. RESULTS AND DISCUSSION

3.1. Indium Oxide Film. We choose indium oxide (In_2O_3) for the channel layer because of the high mobility that results from its large 5 s orbital, which overlaps even in the amorphous phase, its high transparency in the visible region, and from the fact that it is an n-type semiconductor. Moreover, in this study, we used water as a solvent, and film formation was investigated through various analytical tools because formation of aqueous-medium In_2O_3 has rarely been examined in combination with its electrical properties.

To understand the formation of the In_2O_3 film, TG-DTA measurements were performed and the results are shown in Figure 1a. Gradual weight loss was observed up to 330 °C and four endothermic peaks were found. In general, the hydrolysis reaction occurred in the range 100−150 °C. However, in our case, there were no hydrolysis-related peaks because of the In_2O_3 powder preparation temperature of 110 °C; hence, the In_2O_3 powder was already hydrolyzed. The first endothermic peak at 172.5 °C indicates the dehydroxylation behavior of the hydrolyzed indium hydroxide, which reacts with adjacent indium hydroxide molecules and forms an indium oxide lattice. A second peak at 243.7 °C reveals crystallization of the In_2O_3 film, and the other peaks at 280.3 and 318.4 °C may be related to the decomposition of residual nitrate. To verify the above-mentioned chemical reactions, we performed XRD, FT-IR, and XPS measurements.

To clarify the crystalline phase of the In_2O_3 film, XRD measurements were taken as a function of annealing temperature and the results are shown in Figure 1b. The In_2O_3 film shows an amorphous phase up to 230 °C and a crystalline phase was observed at annealing temperatures above 250 °C. The cubic In_2O_3 phase (JCPDS, No. 65−3170) has (200), (222), (400), and (440) peaks at 21.5, 30.6, 35.5, and 50.94°, respectively. This result shows that the aqueous precursor-

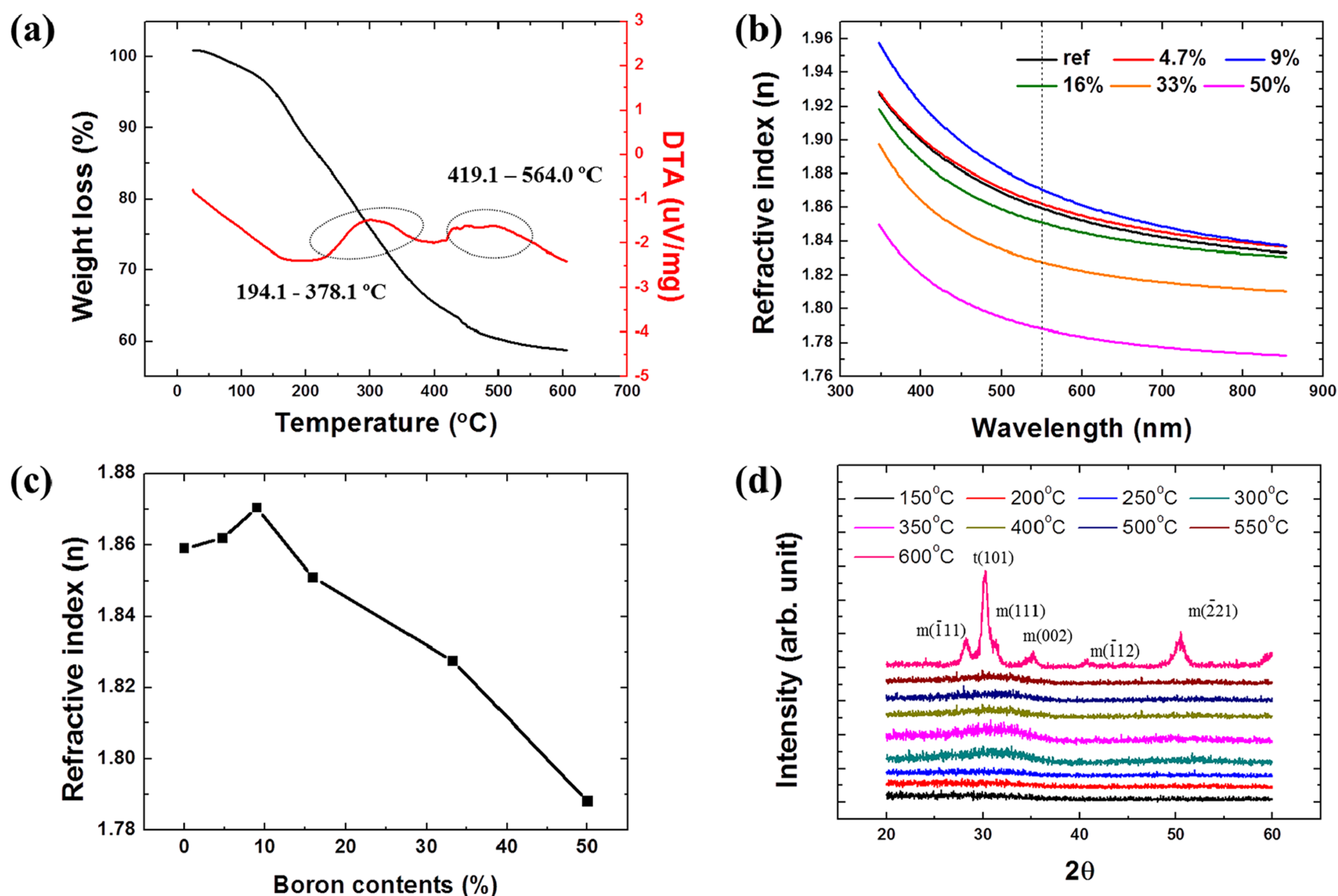

Figure 2. (a) Thermal behavior of 9 mol % boron-doped ZrO_2 powder in ambient air. (b) Refractive index−wavelength curves of 250 °C-annealed ZrO_2 film with various boron concentrations and (c) summarized refractive index values at a wavelength of 550 nm. The 9 mol % boron-doped ZrO_2 film shows the highest refractive index value of 1.851. (d) XRD spectra of ZrO_2:B films with various annealing temperatures. The amorphous ZrO_2:B phase was stabilized up to 550 °C.

derived In_2O_3 thin film crystallized at 250 °C and the DTA peak at 243.7 °C reveals a crystallization endothermic peak.

To better understand the formation of the In_2O_3 film, FT-IR measurements were carried out under various annealing conditions. The O−H stretching vibration shows a broad peak in the range 3000−3500 cm^{-1}.[25] Peaks in the 700−1600 cm^{-1} range indicate hydroxyl groups and a NO_3 deformation vibration.[26] In−O vibration peaks were identified at 597.8, 562.8, and 536.4 cm^{-1}.[27] In the case of 80 °C annealed condition, the In−O bond was not formed and a large number of hydroxyl and nitrate groups remained. The In−O bond was configured at 200 °C and the hydroxyl and nitrate groups gradually decomposed at temperatures up to 300 °C. At annealing temperatures greater than 350 °C, only In−O vibration peaks were observed. Through FT-IR measurement, we found that nitrate groups easily pyrolyzed and In−O bonds formed at 200 °C.

From the TGA and FT-IR results, we found that the gradual weight loss originated from the decomposition of the nitrate and hydroxyl groups. Thus, to confirm the pyrolysis behavior of these groups, we investigated the O 1s and N 1s peaks via XPS. The results are shown in Figure S1 in the Supporting Information and Figure 1d, respectively. A large number of nitrogen peaks were observed in the 80 °C-annealed In_2O_3 film, whereas nitrogen could not be detected in the 350 °C-annealed In_2O_3 film. Three peaks at 399.7, 403.7, and 407 eV were assigned to nitrogen located in the interstitial sites, NO_2, and NO_3, respectively.[28] There was a large amount of nitrogen in the 80 °C-annealed In_2O_3 film, and NO_3-related peaks were undetectable from 230 °C. The NO_2-related peak decreased from 403.7 to 403.4 eV as the annealing temperature increased. This result means that progressive oxidization of the In_2O_3 film with pyrolysis of NO_2 occurred with annealing. Moreover, the peak at 399.7 eV, related to nitrogen located in the interstitial sites, gradually decreased until the annealing temperature reached 300 °C and it could not be detected at 350 °C. This result is comparable to the TGA results, which show a weight loss at temperatures up to 330 °C. The O 1s peak can be divided into three peaks that are centered at 529.8, 531.3, and 532.4 eV, whereas the peaks centered at 529.8 and 531.3 eV can be assigned to oxygen in oxide lattices without oxygen vacancies (O_o) and with oxygen vacancies (O_v), respectively.[29] The peak at 532.4 eV can be assigned to the oxygen in the hydroxide group (O_{OH}). The summarized ratios of $O_o/(O_o+V_o+O_{OH})$, $V_o/(O_o+V_o+O_{OH})$, and $O_{OH}/(O_o+V_o+O_{OH})$ are shown in Figure S2 in the Supporting Information. As the annealing temperature increased, the ratio of $O_{OH}/(O_o+V_o+O_{OH})$ gradually decreased. This result is similar to the FT-IR results, which show a decrease in the number of hydroxyl groups up to 300 °C.

3.2. Boron-Doped Peroxo-Zirconium Oxide. Previously, we reported the fabrication of high-quality peroxo-zirconium oxide (ZrO_2) and we characterized its electrical properties as a gate dielectric.[10] However, its use as a dielectric is restricted to

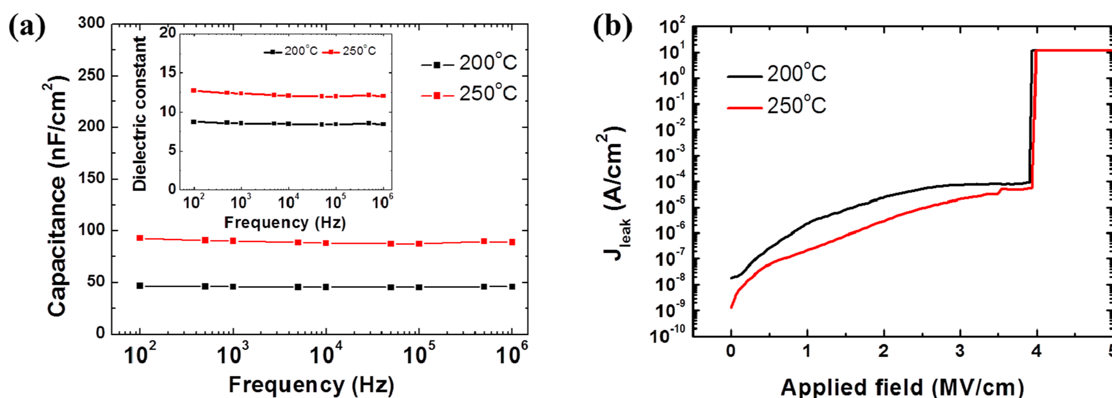

Figure 3. (a) Capacitance−frequency curves of ZrO_2:B films annealed at 200 and 250 °C. Inset indicates dielectric constant of ZrO_2:B film corresponding to its capacitance. (b) J_{leak}-applied field curves of ZrO_2 film annealed at 200 and 250 °C. The figure shows the breakdown voltages of 3.90 and 3.94 MV/cm corresponding to applied voltages of 63.8 and 48.3 V, respectively.

annealing temperatures above 300 °C. Its leakage current densities were 3.5×10^{-5} and 7.3×10^{-8} A/cm^2 at 2 MV/cm at annealing temperatures of 240 and 300 °C, respectively. The essential characteristics of gate dielectrics are a smooth surface that is dense and pinhole-free and has a low-leakage current, a high breakdown voltage, and preferably a high dielectric constant. To realize solution-processed inorganic gate dielectrics on polymer substrates, the annealing temperature should be lower than 200 °C while also satisfying the indispensable characteristics of a gate dielectric. However, forming an inorganic gate dielectric by solution processing is not easy at temperatures below 200 °C and it is rarely reported. To resolve this matter, we made a denser ZrO_2 film by adding boron. The bonding energy of boron to oxygen (B−O) (192.7 kcal/mol) is higher than the bonding energy of zirconium to oxygen (Zr−O) (180.6 kcal/mol).[30,31] Moreover, boric acid acting as a boron dopant source begins to convert to boron oxide at 162 °C.[32] This makes the ZrO_2 film dense, enabling the fabrication of a ZrO_2 film dielectric at low temperature.

The thermal characteristics of the ZrO_2:B powder were investigated and the results are shown in Figure 2a. A gradual weight loss up to 600 °C and two broad exothermic peaks were observed. The first peak in the range 194.1−378.1 °C indicates the dehydroxylation behavior of ZrO_2:B, and the second peak in the range 419.1−564.0 °C indicates crystallization of ZrO_2:B. By adding boron to ZrO_2, the dehydroxylation temperature was slightly decreased and the crystallization temperature was increased as compared with ZrO_2. This means that the boron dopant lowered the dehydroxylation temperature and inhibited the crystallization behavior of the ZrO_2:B film.

To verify these behaviors, we examined the densification and crystallization characteristics of the ZrO_2:B film by using spectroscopic ellipsometry and XRD analysis. Figure 2b shows the refractive index−wavelength curves of the ZrO_2 film with various boron concentrations at 250 °C. As the boron concentration increased up to 9 mol %, the refractive index at a wavelength of 550 nm increased from 1.859 to 1.871. At boron concentrations above 9 mol %, the refractive index of the boron-doped ZrO_2 film decreased from 1.871 to 1.788. This means that boron increases the density of the ZrO_2 film because the ion radius of boron is smaller (r_0 = 41 pm) than that of zirconium (r_0 = 86 pm) and the dehydroxylation temperature of boron hydroxide is lower than that of zirconium hydroxide. As a result, a high ratio of metal−oxygen−metal frame is formed in ZrO_2:B, resulting in a dense film. This behavior is also observed at an annealing temperature of 200 °C (see Figure S3 in the Supporting Information). The 9 mol %-boron-added ZrO_2 film shows the highest refractive index of 1.8 at an annealing temperature of 200 °C. To be used as an insulator for the ZrO_2:B film, the amorphous state is more suitable than the crystalline phase because of its smooth surface and low leakage current density. Grain boundaries in crystalline phases result in leakage paths, such that the device shows high leakage current density.[33] The surface roughness of the 9 mol %-boron-added ZrO_2 film was examined by AFM at various annealing temperatures and the results are shown in Figure S4 in the Supporting Information. The root-mean-square (rms) of the surface roughness for the ZrO_2:B films annealed at 200, 250, 300, and 350 °C were 0.157, 0.145, 0.152, and 0.162 nm, respectively. All of the ZrO_2:B films were very uniform, without a segregation phase, and had a smooth surface with an average surface roughness rms of 0.154 nm.

To investigate the crystallization characteristics of the ZrO_2:B films, we measured the XRD spectra as a function of annealing temperature. The ZrO_2:B films showed an amorphous phase up to 550 °C and crystallization behavior was observed at 600 °C. The crystallized phases of the ZrO_2:B films at 28.2°, 30.1°, 31.2°, 35.2°, 40.66°, and 50.5° indicates m($\bar{1}$11), t(101), m(111), m(002), m($\bar{1}$12), and m($\bar{2}$21), respectively [m, monoclinic phase (JCPDS #37−1484); t, trigonal phase (JCPDS #79−1769)]. All peaks were well-matched with the ZrO_2 phase and no secondary phase such as B_2O_3 was observed. From these results, we confirmed that the exothermic peaks in the range 419.1−564.0 °C indicates crystallization of the ZrO_2:B film. Moreover, boron and peroxo groups stabilized the amorphous ZrO_2 phase until 550 °C. From the results of the thermal and structural measurements, we know that the ZrO_2:B films are dense, smooth, pinhole-free, and amorphous, which satisfies the requirements for gate dielectrics.

The electrical properties of the ZrO_2:B films were measured by using an MIM structure at 200 and 250 °C annealing conditions. The capacitance−frequency curves are shown in figure 3a in the range 100 Hz−1 MHz. The capacitance values of the 200 °C- and 250 °C-annealed ZrO_2:B films are 45.58 ± 0.58 nF/cm^2 and 89.54 ± 1.98 nF/cm^2, respectively. Both films had almost constant capacitance with only a small standard deviation. This means that the ZrO_2:B films contain few hydroxyl groups, which results in high capacitance at low frequency. In general, hydroxyl groups easily adsorb water molecules by electrostatic force. As the number of hydroxyl

groups in the film increases, more water molecules are adsorbed, resulting in high capacitance because of the high dielectric constant of water molecules (ε = 80.1 at 20 °C).[34] Because the ZrO_2:B films have constant capacitance across all frequency ranges, we assume that the ZrO_2:B films were highly oxidized with few hydroxyl groups, even at relatively low annealing temperatures. To verify the presence of hydroxyl groups in the ZrO_2:B film, FT-IR measurements were carried out and the results are shown in Figure S5 in the Supporting Information. The vibration peaks in range 3000−3500 cm^{-1} indicate hydroxyl groups.[25] The peaks at 2944, 2890, and 2831 cm^{-1} indicate C−H stretching vibrations.[35] The range 1300−1500 cm^{-1} represents the asymmetrical stretching vibration of B−O.[36] The solvent-related peaks in the range 1000−1200 cm^{-1} correspond to the stretching vibration mode of the C−O bond. The peroxo group peak corresponding to −O−O− bonds in the ZrO_2 film was assigned at 900 cm^{-1}.[37] The Zr−O bonds were observed at 682, 545, and 470 cm^{-1}.[38] The 80 °C-annealed ZrO_2:B film contained a large number of hydroxyl groups and residual solvent. In the case of the 200 °C-annealed ZrO_2:B film, the number of hydroxyl groups and carbon-related peaks were significantly reduced, and only the ZrO_2:B-related peaks were detected. Through the FT-IR data, we confirmed that the 200 °C-annealed ZrO_2:B film rarely contained hydroxyl groups. The dielectric constants of the ZrO_2:B films annealed at 200 and 250 °C are shown in the inset of Figure 3a. The dielectric constants of the 200 °C- and 250 °C-annealed ZrO_2:B films were 8.48 ± 0.1 and 12.1 ± 0.2, respectively, in all frequency ranges. To utilize the ZrO_2:B film as a gate dielectric, a low leakage current density (J_{leak}) of less than 1 × 10^{-6} A/cm^2 at 1 MV/cm should be acquired. The J_{leak}-applied field curves of the ZrO_2:B films are shown in Figure 3b. The 200 °C- and 250 °C-annealed ZrO_2:B films show J_{leak} values of 2.2 × 10^{-6} and 2.1 × 10^{-7} A/cm^2 at 1MV/cm, respectively, and breakdown voltages of 3.90 and 3.94 MV/cm, respectively, corresponding to applied voltages of 63.8 and 48.3 V. The J_{leak} values of the ZrO_2:B films are reasonable and the breakdown voltages of the applied field are greater than the operating voltage of TFTs. This relative low J_{leak} and high breakdown voltage may originate from the smooth surface, relatively dense film, and high oxidation states with low numbers of hydroxyl groups in the films. In addition, residual chlorine in the ZrO_2:B film also contributes this phenomenon. Actually, 2.1 at % chloride ions remained in the 200 °C annealed ZrO_2:B film. We think that the residual chlorine may passivated defect site in the ZrO_2:B film. In general, halogenated high-k materials exhibit low J_{leak} by decreasing fixed charge, reducing charge trapping, and passivating oxygen vacancy. The oxygen vacancies in the high-*k* materials are main defect site and it leads to conduction path. Thus, reducing oxygen vacancy is important and the residual chlorine in the ZrO_2:B film may passivate the defect sites by accepting nonbonding electrons from undercoordinated Zr ions.[39−42] Therefore, residual chlorine in the ZrO_2:B film results in low J_{leak} at low temperature. These results reveal that the ZrO_2:B films annealed at 200 and 250 °C are suitable for use as gate dielectrics.

3.3. In_2O_3 Thin-Film Transistor on SiO_2/Si^{++} Substrate.

Before integrating an In_2O_3 thin-film transistor combined with a ZrO_2:B dielectric, we investigated the electrical characteristics of In_2O_3 TFTs on thermally grown silicon substrates with 200-nm-thick SiO_2. The gate voltage (V_G)−drain current (I_D) curves of the In_2O_3 TFTs at various annealing temperatures at a drain voltage (V_D) of 40 V are shown in figure 4a. The electrical

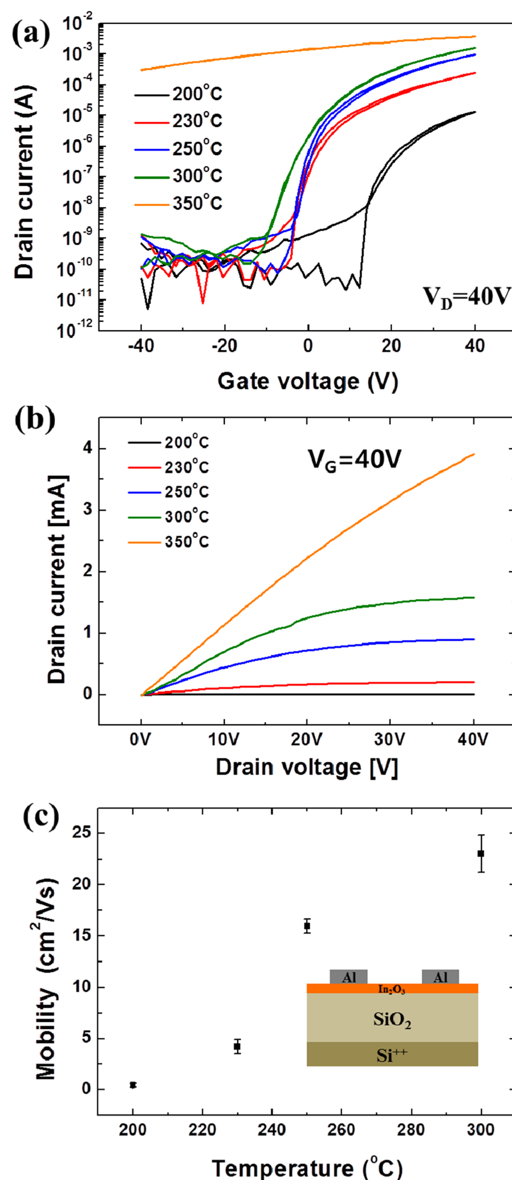

Figure 4. (a) Transfer curves of In_2O_3 TFT on silicon substrate with thermally grown 200-nm-thick SiO_2 at V_D = 40 V as a function of annealing temperature. Hysteresis direction of all transfer curves was clockwise. (b) The output curves of In_2O_3 TFT on SiO_2/Si at V_G = 40 V with a various annealed conditions. (c) Summarized mobility of In_2O_3 TFT on SiO_2/Si substrate. It has a mobility of 0.44 ± 0.15 and 15.95 ± 0.67 cm^2/(V s) at 200 and 250 °C annealing, respectively.

properties of the In_2O_3 TFTs as a function of annealing temperature are summarized in Table 1. All the In_2O_3 TFTs show n-type semiconductor characteristics and clockwise hysteresis directions. The output curves are shown in figure S6 and the summarized output curves at V_G = 40 V are depicted in Figure 4b. The output curve of the saturated drain current for the 300 °C-annealed In_2O_3 TFT with V_G = 40 V was as high as 1.59 mA. The summarized saturation mobility (μ_{sat}) is shown in figure 4c and the inset of Figure 4c indicates the structure of the In_2O_3 TFT on the silicon substrate with 200-nm-thick SiO_2. The μ_{sat} values of the In_2O_3 TFTs annealed at 200, 230, 300, and 350 °C were 0.44 ± 0.15, 4.21 ± 0.67, 15.95 ± 0.67, and 23.04 ± 1.82 cm^2/V·s, respectively. The abrupt increase in μ_{sat} between 230 and 250 °C originated from the crystallization of the In_2O_3 film, as shown in Figure 1b. The crystallized In_2O_3

Table 1. Electrical Properties of In_2O_3 TFT on SiO_2 Dielectric with Various Annealing Conditions

T (°C)	mobility ($cm^2/(V\ s)$)	threshold voltage (V)	on/off current ratio	subthreshold slope (V/dec)	hysteresis (V)
200	0.44 ± 0.15	22.16	4.95×10^5	0.645	1.22
230	4.21 ± 0.67	8.1	2.14×10^6	0.829	1.00
250	15.95 ± 0.67	7.9	5.03×10^6	1.022	0.71
300	23.03 ± 1.82	7.2	7.76×10^6	2.364	0.17
350	conductive				

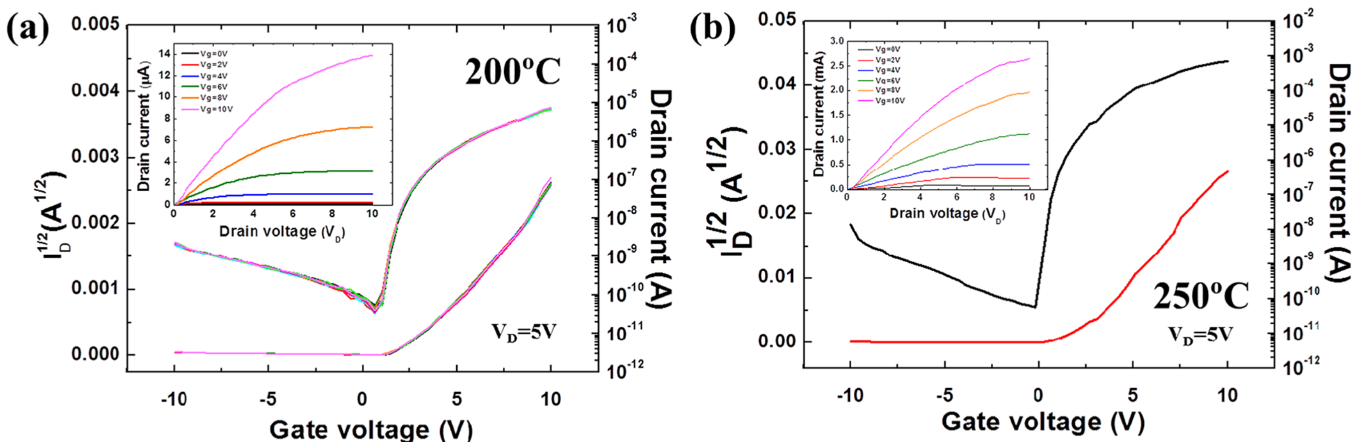

Figure 5. (a) 10× multisweep transfer curves of In_2O_3/ZrO_2:B TFT with V_D = 5 V at 200 °C. Inset indicates output curve of In_2O_3/ZrO_2:B TFT. (b) Transfer curve of In_2O_3/ZrO_2:B TFT with V_D = 5 V at 250 °C. Inset shows the scheme of In_2O_3/ZrO_2:B TFT structure.

film reduces carrier scattering and it may lead to high mobility. The In_2O_3 TFTs showed semiconducting behavior until 300 °C, whereas the 350 °C-annealed In_2O_3 TFT showed conductive characteristics. This feature resulted from the large amount of nitrogen residue in the In_2O_3 film, which suppressed the carrier concentration, leading to low μ_{sat} because nitrogen acted as acceptors in the In_2O_3 film.[43] From the results of the FT-IR and XPS measurement shown in Figure 1c, d, the 200 °C-annealed In_2O_3 film contained large amounts of nitrogen in the film; the amount of nitrogen decreased gradually with increasing annealing temperature. In case of the 350 °C-annealed In_2O_3 film, nitrogen-related peaks were not observed. Thus, the gradual enhancement of μ_{sat} of the In_2O_3 TFTs could be explained by the thermal removal of nitrogen. Moreover, the In_2O_3 precursor derived by the aqueous medium forms In_2O_3 films at low temperature because the water molecules directly participate in the hydrolysis and dehydroxylation reactions. The solution-processed metal oxide synthesized in an organic solvent suffered from the contamination by residual carbon and the presence of carbonyl groups at low annealing temperatures. However, the aqueous In_2O_3 precursor prepared in this study contained only In^{3+}, NO_3^-, and H_2O. The In^{3+} ion is solvated by H_2O and hydrolyzed by forming $In(OH)_3$. $In(OH)_3$ reacts with adjacent $In(OH)_3$ molecules, forming an In−O−In frame. If carbon compounds are used for solvents or additives, the hydrolysis reaction is hindered because of the presence of carbonyl groups, which disturbs the formation of a metal−oxygen−metal frame at low temperatures. On the basis of the results of the In_2O_3 TFTs at various annealing temperatures, it can be deduced that the formation of a metal oxide film by using water as the solvent is promising for low-temperature processes.

3.4. In_2O_3/ZrO_2:B Thin-Film Transistor on Si^{++} Substrate. To demonstrate the feasibility of using ZrO_2:B film as a gate dielectric, we fabricated a bottom-gate structure with a top-contact device on a silicon substrate. Figure 5a shows the 10× swept transfer curves of an amorphous In_2O_3/ZrO_2:B TFT with V_D = 5 V at 200 °C. It has a μ_{sat} of 1.25 $cm^2/(V\ s)$, a V_{th} of 3.89 V, an $I_{on/off}$ of 1.3×10^5, and a subthreshold slope ($S.S$) of 0.313 V/dec The In_2O_3/ZrO_2:B TFT at 200 °C shows good multisweep operating stability and reasonable mobility with good switching characteristics. The inset of Figure 5a shows the output curve of the In_2O_3/ZrO_2:B TFT at 200 °C, and it has clear pinch-off characteristics.

To evaluate the electrical stability of the In_2O_3/ZrO_2:B TFTs at 200 °C, we examined positive gate bias stress for 1000 s at V_G = 5 V. The results are shown in Figure S7 in the Supporting Information. A positive shift of only 0.8 V was observed without changing the $S.S$ values. These results mean that an electron trapping/detrapping mechanism was adopted and trap sites were not generated during stress conditions.[44] An improved dielectric/channel interface trapping site may lead to smaller voltage shifts.

Moreover, we fabricated crystalline-In_2O_3/ZrO_2:B TFTs at 250 °C, and the transfer curves at V_D = 5 V are shown in Figure 5b. The inset of Figure 5b shows the output curves. It has a μ_{sat} of 39.3 $cm^2/(V\ s)$, a V_{th} of 2.46 V, an $I_{on/off}$ of 9.81×10^6, and an $S.S$ of 0.263 V/dec A significant enhancement in mobility was observed. The In_2O_3/ZrO_2:B TFTs annealed at 200 and 250 °C showed mobility enhanced 2−3 times as compared with In_2O_3/SiO_2 TFTs. The origin of the performance enhancement may originate from the enhanced dielectric/channel interface, smooth surface, or high capacitance of the ZrO_2:B film.[45−47]

We have thus successfully demonstrated solution-processed In_2O_3/ZrO_2:B TFT at 200 °C without using complex or expensive equipment. In order to realize solution-processed metal oxide TFTs at low temperatures, most researchers have used a $Zn(OH)_x(NH_3)_y^{(2-x)+}$ precursor for the active layer, an organic gate insulator, and post-treatment.[48−50] However, in this study, we suggest a metal oxide derived from an aqueous

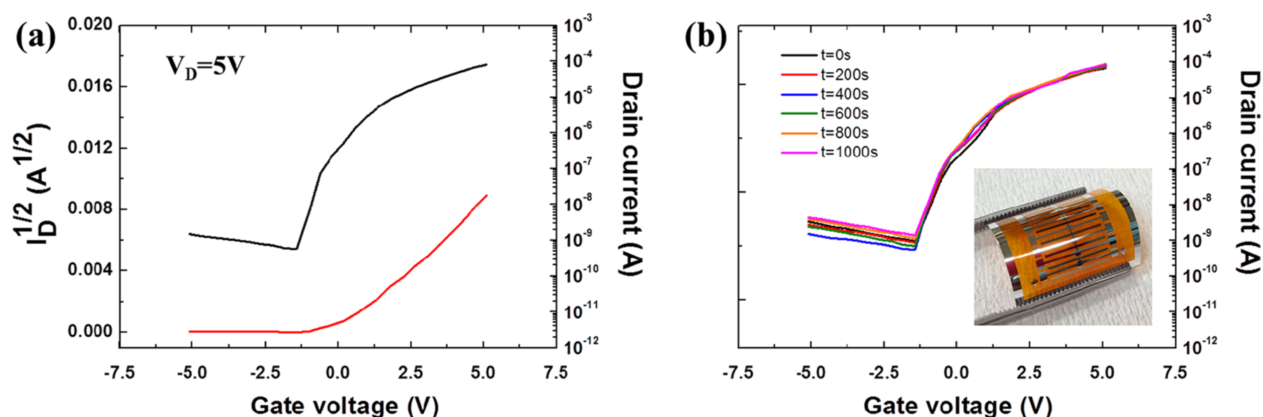

Figure 6. (a) Transfer curves of In_2O_3/ZrO_2:B TFT on PI substrate with V_D = 5 V at 200 °C. (b) Transfer curves of In_2O_3/ZrO_2:B TFT on PI substrate under negative gate bias stress with V_G = 5 V for 1000 s. A shift of only 0.14 V was observed and the inset shows a photograph of the In_2O_3/ZrO_2:B TFT on PI substrate.

medium precursor for the active layer and ZrO_2:B for the dielectric. This method is very simple and reproducible.

3.5. In_2O_3/ZrO_2:B Thin-Film Transistor on Flexible Substrate. Achieving a high-performance oxide device on a flexible substrate is the final goal of the solution process. However, realizing an oxide TFT on a flexible substrate via a solution process has rarely been investigated. The In_2O_3 and ZrO_2:B films researched in this study can be formed at 200 °C and we integrated an In_2O_3/ZrO_2:B TFT on a flexible substrate. The structure of the flexible TFT was Al/In_2O_3/ZrO_2:B/Al on a PVP/PI substrate. The transfer curve of the In_2O_3/ZrO_2:B TFT on PI substrate at V_D = 5 V is shown in figure 6a. The device shows a μ_{sat} of 4.01 $cm^2/(V\ s)$, a V_{th} of 0.28 V, an $I_{on/off}$ of 1.68 × 10^5, and an *S.S* of 0.388 V/dec Furthermore, we investigated the electrical stability of the negative gate bias stress (NBS) for 1000 s at V_G = −5 V. The results are shown in Figure 6b. The electrical stability showed a negative shift of only 0.14 V without changing the *S.S* value. Through the results of an In_2O_3 TFT with a ZrO_2:B dielectric on a PI substrate, we propose that an aqueous medium precursor-derived metal oxide channel and ZrO_2:B dielectric materials are promising for fabricating flexible TFTs.

4. CONCLUSIONS

To realize solution-processed metal oxide TFTs on flexible substrates, we executed material design and analysis using various tools such as TG-DTA, XRD, FT-IR, XPS, and spectroscopic ellipsometry. An aqueous-medium In_2O_3 precursor for the channel material formed In_2O_3 at 200 °C and started to crystallize at 250 °C. To make dense dielectric films, we used a boron dopant in peroxo-zirconium with a 9 mol % concentration. The ZrO_2:B film was highly oxidized at 200 °C and formed a denser film as compared with intrinsic ZrO_2 films. The boron dopant stabilized the amorphous ZrO_2 phase until 550 °C. These dense ZrO_2:B films had uniform dielectric constant values of 8.48 and 12.1 at 200 and 250 °C, respectively, in all frequency ranges, and they effectively blocked J_{leak}. The 200 °C- and 250 °C-annealed ZrO_2:B films showed J_{leak} values of 2.2 × 10^{-6} and 2.1 × 10^{-7} A/cm^2 and breakdown voltages of 3.90 and 3.94 MV/cm. The activation temperature of the In_2O_3/SiO_2 TFT was 200 °C and it had μ_{sat} values of 0.44 and 15.95 $cm^2/(V\ s)$ at 200 and 250 °C, respectively. To evaluate ZrO_2:B as a dielectric, we fabricated an In_2O_3/ZrO_2 TFT on a Si^{++} substrate. The TFT performed successfully with high μ_{sat} values of 1.25 and 39.3 $cm^2/(V\ s)$ at 200 and 250 °C, respectively, and it had good multisweep stability. Finally, we demonstrated the In_2O_3/ZrO_2:B TFT on a PI substrate, and it had a μ_{sat} value of 4.01 $cm^2/(V\ s)$ at 200 °C. Moreover, it showed high NBS stability, with a V_{th} shift of only 0.14 V. The channel layer derived from the aqueous medium precursor and the ZrO_2:B thin film for the dielectric are promising materials for fabricating low-temperature, high-performance, and flexible TFTs.

ASSOCIATED CONTENT

Supporting Information

Cross-sectional SEM image of the ZrO_2:B/Al/PVP/PI substrate. Summarized XPS O 1s peaks of the In_2O_3 film with various annealing conditions. Refractive index−wavelength of the ZrO_2 film with various boron concentrations at 200 °C and summarized refractive index at 550 nm. AFM images of ZrO_2:B films annealed at various temperatures. FT-IR spectra of ZrO_2:B annealed at 80, 200, and 250 °C. Output curves of In_2O_3 TFT on Si substrate with thermally grown 200-nm-thick SiO_2 as a function of annealing temperature. Transfer curves of In_2O_3/ZrO_2 TFT on silicon substrate under positive gate bias stress at V_G = 5 V for 1000 s. This material is available free of charge via the Internet at http://pubs.acs.org.

AUTHOR INFORMATION

Corresponding Author

*E-mail: thinfilm@yonsei.ac.kr. Phone: +82-10-9043-2838.

Notes

The authors declare no competing financial interest.

ACKNOWLEDGMENTS

This work was supported by the National Research Foundation of Korea (NRF, 2012-0008721) funded by the government of Korea (MEST). Further funding came from LG Display.

REFERENCES

(1) Wang, Z. L.; Song, J. *Science* **2006**, *312*, 242−246.
(2) Gozar, A.; Logvenov, G.; Kourkoutis, L. F.; Bollinger, A. T.; Giannuzzi, L. A.; Muller, D. A.; Bozovic, I. *Nature* **2008**, *455*, 782−785.
(3) Nomura, K.; Ohta, H.; Takagi, A.; Kamiya, T.; Hirano, M.; Hosono, H. *Nature* **2004**, *432*, 488−492.
(4) Keimer, B. *Nature* **2006**, *5*, 933−934.

(5) Choi, D.; Choi, M.-Y.; Choi, W. M.; Shin, H.-J.; Park, H.-K.; Seo, J.-S.; Park, J.; Yoon, S.-M.; Chae, S. J.; Lee, Y. H.; Kim, S.-W.; Choi, J.-Y.; Lee, S. Y.; Kim, J. M. *Adv. Mater.* **2010**, *22*, 2187−2192.
(6) Yuhas, B. D.; Yang, P. *J. Am. Chem. Soc.* **2009**, *131*, 3756−3761.
(7) Poizot, P.; Laruelle, S.; Grugeon, S.; Dupont, L.; Tarascon, J.-M. *Nature* **2000**, *407*, 496−499.
(8) Fortunato, E.; Barquinha, P.; Martins, R. *Adv. Mater.* **2012**, *24*, 2945−2986.
(9) Yoo, Y. B.; Park, J. H.; Song, K. M.; Lee, S. J.; Baik, H. K. *J. Sol−Gel Sci. Technol.* **2012**, *64*, 257−263.
(10) Park, J. H.; Yoo, Y. B.; Lee, K. H.; Jang, W. S.; Oh, J. Y.; Chae, S. S.; Baik, H. K. *ACS Appl. Mater. Interfaces* **2013**, *5*, 410−417.
(11) Lee, K. H.; Park, J. H.; Yoo, Y. B.; Jang, W. S.; Oh, J. Y.; Chae, S. S.; Moon, K. J.; Myoung, J. M.; Baik, H. K. *ACS Appl. Mater. Interfaces* **2013**, *5*, 2585−2592.
(12) Park, J. H.; Choi, W. J.; Chae, S. S.; Oh, J. Y.; Lee, S. J.; Song, K. M.; Baik, H. K. *Jpn. J. Appl. Phys.* **2011**, *50*, 080202.
(13) Hwang, Y. H.; Seo, J.-S.; Yun, J. M.; Park, H.; Yang, S.; Park, S.-H. K.; Bae, B.-S. *NPG Asia Mater.* **2013**, *5*, 1−8.
(14) Banger, K. K.; Yamashita, Y.; Mori, K.; Peterson, R. L.; Leedham, T.; Rickard, J.; Sirringhaus, H. *Nat. Mater.* **2011**, *10*, 45−50.
(15) Kim, Y.-H.; Heo, J.-S.; Kim, T.-H.; Park, S.; Yoon, M.-H.; Kim, J.; Oh, M. S.; Yi, G.-R.; Noh, Y.-Y.; Park, S. K. *Nature* **2012**, *489*, 128−132.
(16) Kim, M. G.; Kanatzidis, M. G.; Facchetti, A.; Marks, T. J. *Nat. Mater.* **2011**, *10*, 382−388.
(17) Meyers, S. T.; Anderson, J. T.; Hung, C. M.; Thompson, J.; Wager, J. F.; Keszler, D. A. *J. Am. Chem. Soc.* **2008**, *130*, 17603−17609.
(18) Kim, K. M.; Kim, C. W.; Heo, J.-S.; Na, H.; Lee, J. E.; Park, C. B.; Bae, J.-U.; Kim, C.-D.; Jun, M.; Hwang, Y. K.; Meyers, S. T.; Grenville, A.; Keszler, D. A. *Appl. Phys. Lett.* **2011**, *99*, 242109.
(19) Avis, C.; Kim, Y. G.; Jang, J. *J. Mater. Chem.* **2012**, *22*, 17415−17420.
(20) Kim, S. J.; Yoon, D. H.; Rim, Y. S.; Kim, H. J. *Electrochem. Solid-State Lett.* **2011**, *14*, E35−E37.
(21) Park, J. H.; Lee, S. J.; Lee, T. I.; Kim, J. H.; Kim, C.-H.; Chae, G. S.; Ham, M.-H.; Baik, H. K.; Myoung, J.-M. *J. Mater. Chem. C* **2013**, *1*, 1840−1845.
(22) Xu, X.; Cui, Q.; Jin, Y.; Guo, X. *Appl. Phys. Lett.* **2012**, *101*, 222114.
(23) Yoo, Y. B.; Park, J. H.; Lee, K. H.; Lee, H. W.; Song, K. M.; Lee, S. J.; Baik, H. K. *J. Mater. Chem. C* **2013**, *1*, 1651−1658.
(24) Lin, Y.-H.; Faber, H.; Zhao, K.; Wang, Q.; Amassian, A.; McLachlan, M.; Anthopoulos, T. D. *Adv. Mater.* **2013**, DOI: 10.1002/adma.201301622. Access date: 2013.06.25
(25) Socrates, G. *Infrared Characteristic Group Frequencies: Tables and Charts*, 3rd ed.; John Wiley & Sons: New York, 1994; Vol. *6*, p 94.
(26) Jose, J.; Bushiri, M. J.; Jayakumar, K.; Vaidyan, V. K. *AIP Conf. Proc.* **2008**, *1075*, 125−127.
(27) Rey, J. F. Q.; Plivelic, T. S.; Rocha, R. A.; Tadokoro, S. K.; Torriani, I.; Muccillo, E. N. S. *J. Nanopart. Res.* **2005**, *7*, 203−209.
(28) Reyes-Gil, K. R.; Reyes-Garcıa, E. A.; Raftery, D. *J. Phys. Chem. C* **2007**, *111*, 14579−14588.
(29) Cho, S. Y.; Kang, Y. H.; Jung, J.-Y.; Nam, S. Y.; Lim, J.; Yoon, S. C.; Choi, D. H.; Lee, C. *Chem. Mater.* **2012**, *24*, 3517−3524.
(30) Saritha, D.; Markandeya, Y.; Salagram, M.; Vithal, M.; Singh, A. K.; Bhikshamaiah, G. *J. Non Cryst. Solids* **2008**, *354*, 5573−5579.
(31) Sehon, A. H.; Szwarc, M. *Annu. Rev. Phys. Chem.* **1957**, *8*, 439−462.
(32) Balcı, S.; Sezgi, N. A.; Eren, E. *Ind. Eng. Chem. Res.* **2012**, *51*, 11091−11096.
(33) Chaneliere, C.; Four, S.; Autran, J. L.; Devine, R. A. B.; Sandler, N. P. *J. Appl. Phys.* **1998**, *83*, 4823.
(34) Varghese, O. K.; Grimes, C. A. *J. Nanosci. Nanotechnol.* **2003**, *3*, 277−293.
(35) Socrates, G. *Infrared Characteristic Group Frequencies: Tables and Charts*, 3rd ed.; John Wiley & Sons: New York, 1994; Vol. *6*, p 50.
(36) Deneva, I. M. *J. Univ. Chem. Technol. Metall.* **2010**, *45*, 351−378.
(37) Shearer, J.; Scarrow, R. C.; Kovacs, J. A. *J. Am. Chem. Soc.* **2002**, *124*, 11709−11717.
(38) Agarwal, M.; Guire, M. R. D.; Heuer, A. H. *J. Am. Ceram. Soc.* **1997**, *80*, 2967−2981.
(39) Zheng, J. X.; Ceder, G.; Maxisch, T.; Chim, W. K.; Choi, W. K. *Phys. Rev. B* **2007**, *75*, 104112.
(40) Lai, C. S.; Wu, W. C.; Wang, J. C.; Chao, T. S. *Appl. Phys. Lett.* **2005**, *86*, 222905.
(41) Chen, Y.-T.; Zhao, H.; Wang, Y.; Xue, F.; Zhou, F.; Lee, J. C. *Appl. Phys. Lett.* **2010**, *96*, 103506.
(42) Ha, J.-H.; McIntyre, P. C.; Cho, K. *J. Appl. Phys.* **2007**, *101*, 033706.
(43) Yin, W.; Esposito, D. V.; Yang, S.; Ni, C.; Chen, J. G.; Zhao, G.; Zhang, Z.; Hu, C.; Cao, M.; Wei, B. *J. Phys. Chem. C* **2010**, *114*, 13234−13240.
(44) Schaeffer, J. K.; Gilmer, D. C.; Samavedam, S.; Raymond, M.; Haggag, A.; Kalpat, S.; Steimle, B.; Capasso, C.; White, B. E. *J. Appl. Phys.* **2007**, *102*, 074511.
(45) Nayak, P. K.; Hedhili, M. N.; Cha, D.; Alshareef, H. N. *Appl. Phys. Lett.* **2012**, *100*, 202106.
(46) Wang, L.; Yoon, M. H.; Lu, G.; Yang, Y.; Facchetti, A.; Marks, T. J. *Nat. Mater.* **2006**, *5*, 893−900.
(47) Adamopoulos, G.; Thomas, S.; Wobkenberg, P. H.; Bradley, D. D. C.; McLachlan, M. A.; Anthopoulos, T. D. *Adv. Mater.* **2011**, *23*, 1894−1898.
(48) Jung, Y.; Jun, T.; Kim, A.; Song, K.; Yeo, T. H.; Moon, J. *J. Mater. Chem.* **2011**, *21*, 11879−11885.
(49) Bong, H.; Lee, W. H.; Lee, D. Y.; Kim, B. J.; Cho, J. H.; Cho, K. *Appl. Phys. Lett.* **2010**, *96*, 192115.
(50) Seo, S.-J.; Hwang, Y. H.; Bae, B.-S. *Electrochem. Solid-State Lett.* **2010**, *13*, H357−H359.